Structure of the calcium pyrophosphate monohydrate phase (Ca2P2O7*H2O): towards understanding the dehydration process in calcium pyrophosphate hydrates

Pierre Gras, Nicolas Ratel-Ramond, Sébastien Teychené, Christian Rey, Erik Elkaim, Beatrice Biscans, Stéphanie Sarda, Christèle Combes

Structure of the calcium pyrophosphate monohydrate phase ($Ca_2P_2O_7 \cdot H_2O$): towards understanding the dehydration process in calcium pyrophosphate hydrates

Pierre Gras,[a] Nicolas Ratel-Ramond,[b] Sébastien Teychéné,[c] Christian Rey,[a] Erik Elkaim,[d] Béatrice Biscans,[c] Stéphanie Sarda[e] and Christèle Combes[a]*

[a]CIRIMAT, UMR 5085 INPT–CNRS–UPS, Université de Toulouse, ENSIACET, Toulouse, France, [b]CEMES-CNRS UPR 8011, Toulouse, France, [c]Laboratoire de Génie Chimique, UMR 5503 CNRS–INPT–UPS, Université de Toulouse, Toulouse, France, [d]Synchrotron SOLEIL, L'Orme des Merisiers, Saint-Aubin, Gif-sur-Yvette, France, and [e]CIRIMAT, UMR 5085 INPT–CNRS–UPS, Université de Toulouse and Université Paul Sabatier, Toulouse, France
Correspondence e-mail: christele.combes@ensiacet.fr

Calcium pyrophosphate hydrate (CPP, $Ca_2P_2O_7 \cdot nH_2O$) and calcium orthophosphate compounds (including apatite, octacalcium phosphate *etc.*) are among the most prevalent pathological calcifications in joints. Even though only two dihydrated forms of CPP (CPPD) have been detected *in vivo* (monoclinic and triclinic CPPD), investigations of other hydrated forms such as tetrahydrated or amorphous CPP are relevant to a further understanding of the physicochemistry of those phases of biological interest. The synthesis of single crystals of calcium pyrophosphate monohydrate (CPPM; $Ca_2P_2O_7 \cdot H_2O$) by diffusion in silica gel at ambient temperature and the structural analysis of this phase are reported in this paper. Complementarily, data from synchrotron X-ray diffraction on a CPPM powder sample have been fitted to the crystal parameters. Finally, the relationship between the resolved structure for the CPPM phase and the structure of the tetrahydrated calcium pyrophosphate β phase (CPPT-β) is discussed.

Keywords: crystal structure; calcium pyrophosphate hydrates; powder diffraction; structure determination; pathological calcification; synchrotron study.

1. Introduction

Calcium pyrophosphate hydrate (CPP) and calcium orthophosphate compounds (including apatite, octacalcium phosphate, tricalcium phosphate and whitlockite) are among the most prevalent pathological calcifications in joints (MacMullan *et al.*, 2011). CPP crystals are particularly involved in several kinds of arthritis, including osteoarthritis, a degenerative joint disorder affecting 80% of the population over 75 (Ea *et al.*, 2011). Two different CPP phases have been detected *in vivo* in joints, *viz.* monoclinic and triclinic calcium pyrophosphate dihydrates (CPPD), referred to as m-CPPD and t-CPPD, respectively (Liu *et al.*, 2009). *In vivo* studies have revealed that both are associated with a high inflammatory potential, probably due to their interaction with cell membranes (Roch-Arveiller *et al.*, 1990).

Several other forms of calcium pyrophosphate hydrates have also been synthesized *in vitro*, including two monoclinic calcium pyrophosphate tetrahydrates (CPPT), denoted m-CPPT-α and m-CPPT-β, and an amorphous phase, denoted a-CPP, which has been described as much more stable than the calcium phosphate and calcium carbonate amorphous phases (Brown *et al.*, 1963; Slater *et al.*, 2011).

Although the thermal decomposition of calcium orthophosphates has been studied extensively, few data are available on the behaviour of calcium pyrophosphate hydrates at high temperature. The dehydration process of m-CPPT-β is described as occurring in four steps (Christoffersen *et al.*, 2000; Gras *et al.*, 2013). First, the loss of one water molecule occurs at low temperature ($\sim$323 K) to form a trihydrated calcium pyrophosphate (Gras *et al.*, 2013). This phase was revealed to be highly metastable, rehydration occurring in less than 15 min under normal conditions of humidity at room temperature. The second step in the dehydration process corresponds to the loss of two water molecules at around 373 K to form calcium pyrophosphate monohydrate (CPPM). The next dehydration step involves the formation of a calcium orthophosphate phase, monetite $CaHPO_4$, by hydrolysis of the pyrophosphate molecules, and the final step is condensation into anhydrous β-$Ca_2P_2O_7$. The structures of the tri- and monohydrated phases were described in the earlier works, but a full understanding of the different steps in the dehydration of CPP hydrates, particularly the involvement of hydrolysis reactions of the pyrophosphate molecules, is still lacking.

The present study focuses on the structure of calcium pyrophosphate monohydrate resolved by single-crystal X-ray diffraction (XRD) as a key step to further understanding the m-CPPT-β dehydration process. The preparation of CPPM crystals by diffusion in gel is also described.

2. Experimental

2.1. Synthesis and crystallization

The technique used for the synthesis of hydrated CPP single crystals consists of the diffusion of separate calcium and pyrophosphate solutions into a silica gel, leading to a sufficiently high supersaturation in the gel to initiate homogeneous nucleation and slow growth of calcium pyrophosphate crystals. The gel method of crystal growth is often used for single-crystal synthesis because of its simplicity and the quality of the crystals produced, which are suitable for single-crystal characterization (Tamain *et al.*, 2012).

doi:10.1107/S2053229614017446

Anhydrous tetrasodium pyrophosphate ($Na_4P_2O_7$) was obtained by heating disodium hydrogen phosphate (Na_2HPO_4, 100 g, Merck, >99% purity) in a muffle furnace at 673 K for 3 h. Calcium chloride ($CaCl_2$, Merck, >95% purity), acetic acid solution (VWR, 100% purity) and sodium metasilicate pentahydrate ($Na_2SiO_3{\cdot}5H_2O$, Aldrich, >95% purity) were used as received without further purification. All solutions were prepared using deionized water.

The diffusion cell implemented for the present study was composed of three compartments with the same volume (150 ml), each separated by a dialysis membrane. The gel was prepared by adding sodium metasilicate pentahydrate ($Na_2SiO_3{\cdot}5H_2O$, 25 g) to deionized water (300 ml); the gel obtained had a density of 1.04 Mg m^{-3} (Deepa *et al.*, 1994). After complete dissolution, the metasilicate solution was added continuously with stirring (400 r min^{-1}) to acetic acid (15 ml) at a constant volumetric flow rate (7.25 ml min^{-1}) using a peristaltic pump. The alkaline metasilicate was added until the pH of the final solution reached 5.8. The addition of the solution to the acid with stirring avoided the formation of inhomogeneities in the gel microenvironment. The solution was then poured into the central compartment of the diffusion cell, delimited on both sides by a dialysis membrane (Cellu Step T3, MWCO 12000-14000), and a homogeneous gel was obtained after 48 h of maturation.

The calcium and pyrophosphate reagent solutions were prepared separately by dissolving $CaCl_2$ (13.88 g, 12.50 × 10^{-2} mol) and $Na_4P_2O_7$ (16.62 g, 6.25 × 10^{-2} mol) in deionized water (250 ml). Each solution was poured into one side compartment of the cell. The system was then kept undisturbed for two weeks at room temperature.

m-CPPT-β crystal spherulites were formed with a diameter of around 1 mm, containing crystals large enough for X-ray characterization. The crystals showed a thin platelet morphology with an orientation perpendicular to [100]. These large crystals of m-CPPT-β were then heated at 383 K for 30 min, resulting in their dehydration into the monoclinic calcium pyrophosphate monohydrate phase (m-CPPM).

2.2. Refinement

Crystal data, data collection and structure refinement details are summarized in Table 1. The selected crystal of m-CPPM was mounted on a Microloop (MiTeGen) using perfluoropolyether oil and cooled rapidly to 180 K in a stream of cold N_2. However, owing to the small size and rather poor quality of the m-CPPM crystals that were obtained by heating m-CPPT-β crystals at 383 K for 30 min, large and elongated reflections were registered, limiting the accuracy of the structural parameters. The position of H atoms were determined using Fourier difference maps and all H-atom parameters were refined freely.

Complementarily, we checked that the data (the structural parameters) obtained from single-crystal XRD fitted the X-ray powder diffraction data collected on the Cristal beamline at the SOLEIL synchrotron (Gif-sur-Yvette, France; http://www.synchrotron-soleil.fr/). A monochromatic beam was selected using an Si(111) double-crystal monochromator and its wavelength (0.72442 Å) determined using NIST standard LaB_6. The powder sample was placed in a 0.7 mm diameter glass capillary, mounted on a spinner to improve averaging. High angular resolution was obtained with the 21 (*i.e.* 21 diffraction patterns in a single acquisition) perfect-crystal Si(111) rear analyser mounted on a two-circle diffractometer.

The powder diffraction pattern was indexed using the LSI method implemented in *TOPAS* (Coelho, 2003, 2009) in a monoclinic system of setting $P2_1/n$ or $P2_1/c$. The Rietveld refinement was performed using *JANA2006* (Petříček *et al.*, 2006).

Table 1
Experimental details.

Crystal data	
Chemical formula	$Ca_2P_2O_7{\cdot}H_2O$
M_r	272.12
Crystal system, space group	Monoclinic, $P2_1/n$
Temperature (K)	180
a, b, c (Å)	10.16 (14), 6.97 (5), 10.77 (10)
β (°)	114.4 (4)
V (Å^3)	695 (12)
Z	4
Radiation type	Mo $K\alpha$
μ (mm^{-1})	2.11
Crystal size (mm)	0.2 × 0.03 × 0.02
Data collection	
Diffractometer	Bruker Kappa APEXII diffractometer with a Quasar CCD area-detector
Absorption correction	Multi-scan (*SADABS*; Bruker, 2001)
T_{min}, T_{max}	0.665, 0.957
No. of measured, independent and observed [$I > 2\sigma(I)$] reflections	7104, 1402, 996
R_{int}	0.059
(sin $\theta/\lambda)_{max}$ (Å^{-1})	0.625
Refinement	
$R[F^2 > 2\sigma(F^2)]$, $wR(F^2)$, S	0.051, 0.133, 1.06
No. of reflections	1402
No. of parameters	117
H-atom treatment	All H-atom parameters refined
$\Delta\rho_{max}$, $\Delta\rho_{min}$ (e Å^{-3})	0.89, −0.69

Computer programs: *APEX2* (Bruker, 2007), *SAINT* (Bruker, 2007), *SORTAV* (Blessing, 1995), *SHELXS97* (Sheldrick, 2008), *SHELXL2014* (Sheldrick, 2014) and *WinGX* (Farrugia, 2012).

3. Results and discussion

The XRD data obtained from the single-crystal analysis led to the refined cell constants and additional crystal data reported in Table 1. The resolved molecular structure for the CPPM phase is presented in Fig. 1. Selected bond lengths are reported in Table 2.

The reciprocal lattice corresponds to a monoclinic system, with systematic extinctions consistent with the space group $P2_1/n$, similar to the space group of the m-CPPT-β structure determined by Balić-Žunić *et al.* (2000), and its asymmetric unit contains only one unit, $Ca_2P_2O_7{\cdot}H_2O$.

We checked the structure determined from single-crystal XRD data by using a refinement of synchrotron X-ray powder diffraction data for the m-CPPM sample (Fig. 2). The unit-cell

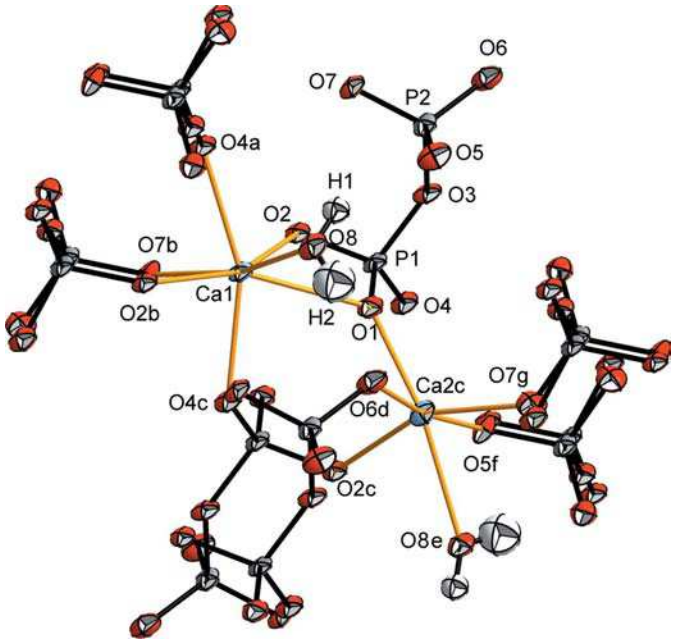

Figure 1
The molecular structure of m-CPPM, showing the atom-numbering scheme and symmetry-equivalent atoms. Displacement ellipsoids are drawn at the 50% probability level, except for H atoms, which are represented by 20% probability spheres. [Symmetry codes: (*a*) $x+\frac{1}{2}, -y+\frac{1}{2}, z+\frac{1}{2}$; (*b*) $-x+\frac{3}{2}, y+\frac{1}{2}, -z+\frac{3}{2}$; (*c*) $-x+1, -y+1, -z+1$; (*d*) $x, y+1, z$; (*e*) $x-\frac{1}{2}, -y+\frac{3}{2}, z-\frac{1}{2}$; (*f*) $-x+\frac{1}{2}, y+\frac{1}{2}, -z+\frac{3}{2}$; (*g*) $x-\frac{1}{2}, -y+\frac{1}{2}, z-\frac{1}{2}$.]

parameters obtained were a = 10.0058 (5) Å, b = 6.8629 (3) Å, c = 10.5596 (5) Å and β = 114.258 (2)°. The unit cell for the $P2_1/c$ space group was obtained using the transformation matrix (001/010/$\overline{1}0\overline{1}$) and refined with cell parameters a = 10.5596 (4) Å, b = 6.8630 (2) Å, c = 11.1762 (5) Å and β = 125.257 (2)°, for comparison with the m-CPPT-β structure. The structure was fully resolved and refined. The results were in good agreement with the structure obtained by single-crystal XRD analysis.

We note that the resolved structure for m-CPPM is closely related to that of m-CPPT-β (Fig. 3). The structure of m-CPPT-β is formed by alternate layers of water molecules and calcium pyrophosphate oriented in the (100) plane (Balić-Žunić *et al.*, 2000). In this structure, two different layers are linked together only by hydrogen bonds. In a second framework, the inner layer of calcium pyrophosphate can also be described as constituting layers of calcium and layers of pyrophosphate organized in the (001) plane, transverse to the water layers (Fig. 3*a*). This organization can be compared with that of brushite ($CaHPO_4{\cdot}2H_2O$), described as a layered

Table 2
Selected bond lengths (Å).

Ca1—O7^{i}	2.37 (2)	Ca2—O1^{ii}	2.388 (18)
Ca1—O2^{i}	2.389 (16)	Ca2—O7^{i}	2.427 (18)
Ca1—O4^{ii}	2.410 (14)	Ca2—O8^{v}	2.554 (16)
Ca2—O5^{iii}	2.33 (3)	Ca2—O3^{iv}	2.968 (18)
Ca2—O6^{iv}	2.34 (2)		

Symmetry codes: (i) $-x+\frac{3}{2}, y+\frac{1}{2}, -z+\frac{3}{2}$; (ii) $-x+1, -y+1, -z+1$; (iii) $x+\frac{1}{2}, -y+\frac{1}{2}, z-\frac{1}{2}$; (iv) $-x+1, -y, -z+1$; (v) $-x+\frac{3}{2}, y-\frac{1}{2}, -z+\frac{3}{2}$.

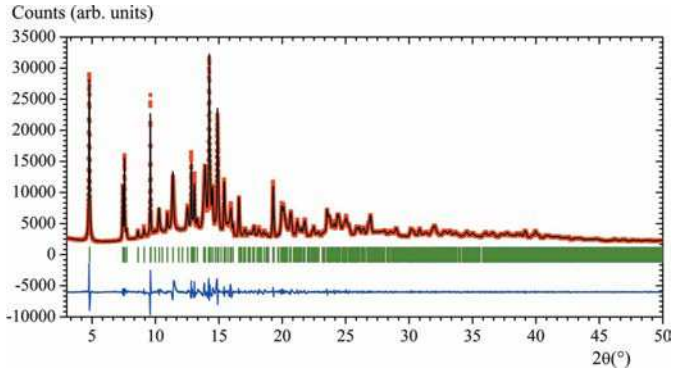

Figure 2
Rietveld plot for the m-CPPM phase based on the powder XRD pattern. Observed data points are indicated by dots, and the best-fit profile (upper trace) and the difference pattern (lower trace) are solid lines. The vertical bars indicate the positions of the Bragg peaks.

structure in which the layers are held together by water molecules *via* hydrogen bonding (Dosen & Giese, 2011). The dehydration of brushite leads to the formation of monetite, $CaHPO_4$; these two calcium orthophosphate phases have the same Ca/P atomic ratio as the m-CPPM and m-CPPT-β calcium pyrophosphate phases.

It has been shown by Balić-Žunić *et al.* (2000) that partial dehydration of m-CPPT-β involves the release of three water molecules, referred to as O*W*2, O*W*3 and O*W*4. These water molecules are held in the m-CPPT-β structure either by a weak interaction with Ca2 (O*W*2 and O*W*3) or by hydrogen bonds only (O*W*4). They were described as being weakly bound compared with atom O8, which is coordinated to both Ca1 and Ca2. The dehydrated structure loses its initial layered organization based on hydrogen bonds with water molecules, with a closing of the gap resulting in the formation of bonds between the pyrophosphate molecules and calcium, as observed in the m-CPPM structure. The layered framework of calcium and pyrophosphate still remains in the (001) plane, but is slightly modified.

The transition between these inner calcium pyrophosphate structures could be described as a reorganization of the calcium (001) framework, related to the formation of the Ca2—O5 coordination between the different layers. The Ca layer is inclined at 2.2° relative to (001) in m-CPPM, compared with an inclination of 11.5° for m-CPPT-β. The Ca2—O5 coordination is created in the former water layers and, as a consequence, the inner layered structure is slightly modified by this reorientation. Atoms Ca1 and P1, in particular, keep almost the same structural environment in m-CPPM as in m-CPPT-β, on the 2_1 axes for Ca1 and on the *c*-glide for P1.

This deformation, supposedly based on the orientation of the calcium framework, leads to greater deformations of the P2 tetrahedron of the pyrophosphate molecules. It also involves a change in the Ca2 environment, which evolves from coordination polyhedra with a coordination number of 7 (CN7) to new ones with CN6. CN6 has not yet been observed for hydrated calcium pyrophosphate, but it is common for anhydrous calcium pyrophosphates β-$Ca_2P_2O_7$, other hydrated pyrophosphate compounds ($X_2P_2O_7{\cdot}2H_2O$; X = Mg, Mn,

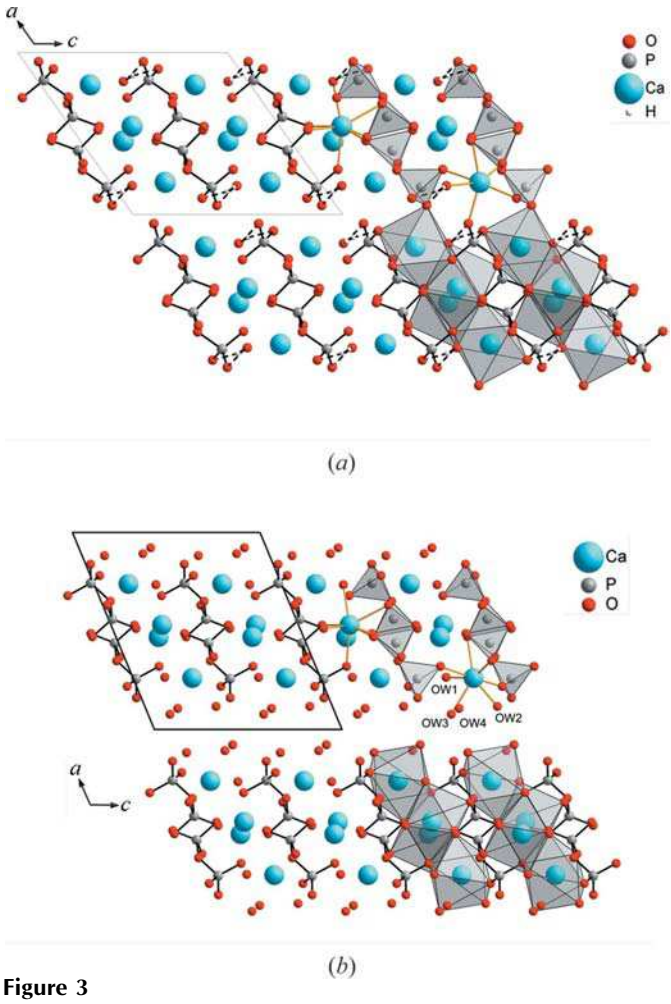

Figure 3
Comparison of projections along the *b* axis of (*a*) the structure of m-CPPM, showing the polyhedron frameworks in the structure with $P2_1/c$ symmetry (dashed lines indicate hydrogen bonds), and (*b*) the structure of m-CPPT-β.

Fe, Co) or calcium phosphate hydrates like octacalcium phosphate, and could explain the dehydration mechanism without a major reorganization. The loss of water molecules O*W*2 and O*W*3 and the formation of the Ca2—O5 coordination deforms the Ca2 coordination polyhedra.

The new coordination provides the only link between the former calcium pyrophosphate layers, the remaining hydrogen bond of O8 being reoriented to the closest pyrophosphates on the same side of the initial gap between the calcium pyrophosphate layers. As a consequence, the Ca2 polyhedron is a highly distorted octahedron, resembling a pentagonal bipyramid with a missing O atom due to dehydration. Indeed, atom O5 takes a position between the former O*W*2 and O*W*3 positions in the coordination sphere, closer to the O*W*3 position. Water molecule O*W*3 has already been reported by Balić-Žunić *et al.* (2000) to face atom O5 with matching surfaces. The Ca2 distorted octahedron has an O6—Ca2—O7 [171.85 (18)°] axis to which the equatorial O1—O2—O5—O8 plane is nearly perpendicular [87.3 (15)°]. The angles between the Ca2—O bonds show the initial position of the water molecules by virtue of a larger distortion at that position: 78.5 (7) (O8—Ca2—O5), 78.6 (8) (O8—Ca2—O2), 80.1 (6) (O2—Ca2—O1) and 119.5 (6)° (O5—Ca2—O1). The next closest O atom in the m-CPPM structure is O3 at 2.97 (4) Å, but this cannot be considered part of the Ca2 coordination environment, due to its distance and position as a bridging atom in the pyrophosphate molecule.

In the m-CPPM structure, the Ca atoms of parallel Ca chains are surrounded by oxygen polyhedra sharing O–O edges. Atom O1 is a shared vertex between the Ca1 polyhedron at (x, y, z) and the Ca2 polyhedron at ($-x+1$, $-y+1$, $-z+1$), resulting in a Ca chain. The orientations of the pyrophosphate molecules, defined by the P1···P2 vector, are alternately parallel to [0$\bar{1}$1] and [01$\bar{1}$] in a complementary structure.

Pyrophosphate molecules are reported to have a very high flexibility with two characteristic configurations, staggered or eclipsed (Rulmont *et al.*, 1991). Similar to pyrosilicates, pyroarsenates or pyrogermanates, crystals of pyrophosphate compounds of the composition $X_2P_2O_7$, with an ionic radius of X less than 0.97 Å (X = Mg, Mn, Fe, Co, Ni, Cu, Zn), are isostructural with thortveitite ($Sc_2Si_2O_7$), with the P—O—P bond angle varying from 140 to 180°, an O—P···P—O pseudo-torsion angle of 60° (staggered conformation) and the YO_4 (Y = P, Si, As, Ge) tetrahedra showing a very low degree of distortion. For an ionic radius greater than 0.97 Å (X = Ca, Sr, Ba) or for hydrates, pyrophosphate molecules usually have the same configuration as the dichromate structure, with a P—O—P angle of approximately 120–135°, an O—P···P—O pseudo-torsion angle of 0–30° (eclipsed conformation) and distorted YO_4 (Y = P, Si, As, Ge) tetrahedra (Davis *et al.*, 1985). In the present structure of m-CPPM, the angle of the P—O—P bridge, the torsion between the two phosphate tetrahedra and the P—O3 distance correspond to an eclipsed configuration. The evolution of this structure leads to a highly deformed P2 tetrahedron for m-CPPM, with the P2—O3 distance, 1.680 (16) Å, being the highest reported to date. The two tetrahedra have the same orientation, with a difference between the O4/O1/O3 and O6/O5/O3 bases of the phosphate group of 12.2 (3)° and a O4—P1···P2—O6 torsion angle of 4.9 (6)° [this torsion is defined by Mandel (1975) and the choice is based on the orientation of the central O atom]. For comparison, the angle between the two terminal phosphate groups for m-CPPT-β is 19.6° and the torsion angle is 9.1°. Finally, the P1—O3—P1 angle in m-CPPM is 132.7 (4)°, compared with 134.1° for m-CPPT-β.

Dehydration leads to a higher density, from 2.36 Mg m^{-3} for m-CPPT-β to 2.60 Mg m^{-3} for m-CPPM. The volume of the cell also decreases by 25%, from 918.4 to 695 (12) Å^3.

The distance between atoms O8 and O3 in the m-CPPM structure is 3.21 (4) Å. The water molecule is close to the central O atom of the pyrophosphate molecule. This configuration could favour the internal hydrolysis of pyrophosphate ions into hydrogenphosphate ions. This would contribute to our understanding of the hydrolysis phenomenon occurring during the next step in the dehydration of the m-CPPM phase.

The next step that occurs upon heating m-CPPM corresponds, unexpectedly, to the transient hydrolysis of pyro-

phosphate ions and the formation of monetite ($CaHPO_4$). At higher temperatures, condensation of the hydrogen phosphate re-forms the pyrophosphate ions, *i.e.* β-$Ca_2P_2O_7$, and completes the dehydration process.

The authors thank Nathalie Saffon from the Service Commun Rayons X of the Institut de Chimie de Toulouse ICT-FR2599 (Université Paul Sabatier, Toulouse, France) for the single-crystal X-ray diffraction analysis, SOLEIL for the provision of synchrotron radiation facilities (proposal No. 20130932, Cristal beamline) and the Agence Nationale de la Recherche (CAPYROSIS project No. ANR-12-BS08–0022-01) for supporting this research work.

References

Balić-Žunić, T., Christoffersen, M. R. & Christoffersen, J. (2000). *Acta Cryst.* B**56**, 953–958.
Blessing, R. H. (1995). *Acta Cryst.* A**51**, 33–38.
Brown, E. H., Lehr, J. R., Smith, J. P. & Frazier, A. W. (1963). *J. Agric. Food. Chem.* **11**, 214–222.
Bruker (2001). *SADABS*. Bruker AXS Inc., Madison, Wisconsin, USA.
Bruker (2007). *APEX2* and *SAINT*. Bruker AXS Inc., Madison, Wisconsin, USA.
Christoffersen, M. R., Balić-Žunić, T., Pehrson, S. & Christoffersen, J. (2000). *J. Cryst. Growth*, **212**, 500–506.
Coelho, A. A. (2003). *J. Appl. Cryst.* **36**, 86–95.
Coelho, A. A. (2009). *TOPAS-Academic*. Coelho Software, Brisbane, Australia.
Davis, N. L., Mandel, G. S., Mandel, N. S. & Dickerson, R. E. (1985). *J. Crystallogr. Spectrosc. Res.* **15**, 513–521.
Deepa, M., Rajendra Babu, K. & Vaidyan, V. K. (1994). *Bull. Mater. Sci.* **17**, 105–110.
Dosen, A. & Giese, R. F. (2011). *Am. Mineral.* **96**, 368–373.
Ea, H.-K., Nguyen, C., Bazin, D., Bianchi, A., Guicheux, J., Reboul, P., Daudon, M. & Lioté, F. (2011). *Arthritis Rheum.* **63**, 10–18.
Farrugia, L. J. (2012). *J. Appl. Cryst.* **45**, 849–854.
Gras, P., Teychené, S., Rey, C., Charvillat, C., Biscans, B., Sarda, S. & Combes, C. (2013). *CrystEngComm*, **15**, 2294–2300.
Liu, Y. Z., Jackson, A. P. & Cosgrove, S. D. (2009). *Osteoarthritis Cartilage*, **17**, 1333–1340.
MacMullan, P., McMahon, G. & McCarthy, G. (2011). *Joint Bone Spine*, **78**, 358–363.
Mandel, N. S. (1975). *Acta Cryst.* B**31**, 1730–1734.
Petříček, V., Dušek, M. & Palatinus, L. (2006). *JANA2006*. Institute of Physics, Czech Academy of Sciences, Prague, Czech Republic.
Roch-Arveiller, M., Legros, R., Chanaud, B., Muntaner, O., Strzalko, S., Thuret, A., Willoughby, D. A. & Giroud, J. P. (1990). *Biomed. Pharmacother.* **44**, 467–474.
Rulmont, A., Cahay, R., Liegeois-Duyckaerts, M. & Tarte, P. (1991). *Eur. J. Solid State Inorg. Chem.* **28**, 207–219.
Sheldrick, G. M. (2008). *Acta Cryst.* A**64**, 112–122.
Sheldrick, G. M. (2014). *SHELXL2014*. University of Göttingen, Germany.
Slater, C., Laurencin, D., Burnell, V., Smith, M. E., Grover, L. M., Hriljac, J. A. & Wright, A. J. (2011). *J. Mater. Chem.* **21**, 18783–18791.
Tamain, C., Arab-Chapelet, B., Rivenet, M., Abraham, F. & Grandjean, S. (2012). *Cryst. Growth Des.* **12**, 5447–5455.

supporting information

Structure of the calcium pyrophosphate monohydrate phase ($Ca_2P_2O_7 \cdot H_2O$): towards understanding the dehydration process in calcium pyrophosphate hydrates

Pierre Gras, Nicolas Ratel-Ramond, Sébastien Teychéné, Christian Rey, Erik Elkaim, Béatrice Biscans, Stéphanie Sarda and Christèle Combes

Computing details

Data collection: *APEX2* (Bruker, 2007); cell refinement: *SAINT* (Bruker, 2007); data reduction: *SORTAV* (Blessing, 1995); program(s) used to solve structure: *SHELXS97* (Sheldrick, 2008); program(s) used to refine structure: *SHELXL2014* (Sheldrick, 2014).

Calcium pyrophosphate monohydrate

Crystal data

$Ca_2P_2O_7 \cdot H_2O$
$M_r = 272.12$
Monoclinic, $P2_1/n$
Hall symbol: -P 2yn
$a = 10.16$ (14) Å
$b = 6.97$ (5) Å
$c = 10.77$ (10) Å
$\beta = 114.4$ (4)°
$V = 695$ (12) Å^3
$Z = 4$
$F(000) = 544$
$D_x = 2.602$ Mg m^{-3}
Mo $K\alpha$ radiation, $\lambda = 0.71073$ Å
Cell parameters from 1804 reflections
$\theta = 3.7$–$27.8°$
$\mu = 2.11$ mm^{-1}
$T = 180$ K
Needle, colourless
0.2 × 0.03 × 0.02 mm

Data collection

Bruker Kappa APEXII diffractometer with Quasar CCD area-detector
Radiation source: micro-focus
Multilayer optics monochromator
φ and ω scans
Absorption correction: multi-scan (*SADABS*; Bruker, 2001)
$T_{min} = 0.665$, $T_{max} = 0.957$
7104 measured reflections
1402 independent reflections
996 reflections with $I > 2\sigma(I)$
$R_{int} = 0.059$
$\theta_{max} = 26.4°$, $\theta_{min} = 5.3°$
$h = -12 \rightarrow 12$
$k = -8 \rightarrow 8$
$l = -13 \rightarrow 13$

Refinement

Refinement on F^2
Least-squares matrix: full
$R[F^2 > 2\sigma(F^2)] = 0.051$
$wR(F^2) = 0.133$
$S = 1.06$
1402 reflections
117 parameters
0 restraints
Primary atom site location: structure-invariant direct methods
Secondary atom site location: difference Fourier map
Hydrogen site location: inferred from neighbouring sites

All H-atom parameters refined
$w = 1/[\sigma^2(F_o^2) + (0.0566P)^2 + 4.017P]$
where $P = (F_o^2 + 2F_c^2)/3$

$(\Delta/\sigma)_{max} < 0.001$
$\Delta\rho_{max} = 0.89$ e Å^{-3}
$\Delta\rho_{min} = -0.69$ e Å^{-3}

Special details

Geometry. All e.s.d.'s (except the e.s.d. in the dihedral angle between two l.s. planes) are estimated using the full covariance matrix. The cell e.s.d.'s are taken into account individually in the estimation of e.s.d.'s in distances, angles and torsion angles; correlations between e.s.d.'s in cell parameters are only used when they are defined by crystal symmetry. An approximate (isotropic) treatment of cell e.s.d.'s is used for estimating e.s.d.'s involving l.s. planes.

Fractional atomic coordinates and isotropic or equivalent isotropic displacement parameters (Å²)

	x	*y*	*z*	U_{iso}*/U_{eq}
O1	0.4356 (5)	0.4417 (6)	0.6198 (4)	0.0238 (10)
O2	0.6208 (4)	0.2267 (6)	0.5986 (4)	0.0179 (9)
O3	0.4099 (4)	0.0743 (6)	0.6350 (4)	0.0205 (10)
O4	0.3620 (4)	0.2220 (6)	0.4061 (4)	0.0220 (10)
O5	0.4312 (5)	0.1701 (7)	0.8751 (4)	0.0304 (11)
O6	0.3854 (5)	−0.1793 (7)	0.7846 (5)	0.0282 (11)
O7	0.6306 (4)	−0.0269 (7)	0.8522 (4)	0.0235 (10)
O8	0.5937 (5)	0.5446 (9)	0.9158 (5)	0.0264 (11)
P1	0.45546 (16)	0.2487 (2)	0.56019 (15)	0.0184 (4)
P2	0.46790 (17)	0.0080 (2)	0.79898 (15)	0.0200 (4)
Ca1	0.70409 (13)	0.51047 (18)	0.74953 (12)	0.0186 (3)
Ca2	0.73672 (14)	0.3039 (2)	0.43544 (13)	0.0242 (4)
H1	0.572 (10)	0.421 (15)	0.905 (9)	0.05 (3)*
H2	0.526 (13)	0.631 (19)	0.885 (12)	0.10 (4)*

Atomic displacement parameters (Å²)

	U^{11}	U^{22}	U^{33}	U^{12}	U^{13}	U^{23}
O1	0.023 (2)	0.022 (2)	0.018 (2)	0.0011 (19)	−0.0002 (19)	−0.0022 (19)
O2	0.018 (2)	0.019 (2)	0.0101 (19)	0.0007 (17)	−0.0011 (17)	0.0001 (17)
O3	0.021 (2)	0.021 (2)	0.011 (2)	−0.0021 (19)	−0.0020 (17)	−0.0002 (18)
O4	0.020 (2)	0.024 (3)	0.012 (2)	0.0000 (19)	−0.0039 (17)	0.0001 (18)
O5	0.033 (3)	0.035 (3)	0.017 (2)	0.005 (2)	0.005 (2)	−0.003 (2)
O6	0.024 (2)	0.026 (3)	0.024 (2)	−0.005 (2)	−0.0012 (19)	0.001 (2)
O7	0.016 (2)	0.033 (3)	0.013 (2)	0.0016 (19)	−0.0030 (17)	0.0048 (19)
O8	0.023 (3)	0.030 (3)	0.017 (2)	0.000 (2)	−0.0017 (19)	−0.004 (2)
P1	0.0146 (8)	0.0196 (8)	0.0115 (7)	−0.0007 (7)	−0.0041 (6)	−0.0011 (6)
P2	0.0166 (8)	0.0233 (9)	0.0135 (8)	−0.0003 (7)	−0.0003 (6)	−0.0004 (7)
Ca1	0.0163 (6)	0.0191 (7)	0.0126 (6)	−0.0009 (5)	−0.0020 (5)	−0.0005 (5)
Ca2	0.0192 (6)	0.0315 (8)	0.0141 (6)	0.0024 (6)	−0.0008 (5)	−0.0004 (6)

Geometric parameters (Å, º)

O1—P1	1.540 (10)	P2—Ca2^{iii}	3.33 (2)
O1—Ca2^{i}	2.388 (18)	P2—Ca2^{ii}	3.48 (3)
O1—Ca1	2.54 (3)	P2—Ca2^{v}	3.50 (3)

O2—P1	1.56 (2)	Ca1—O7^{vi}	2.37 (2)
O2—Ca1^{ii}	2.389 (16)	Ca1—O2^{vi}	2.389 (16)
O2—Ca1	2.476 (14)	Ca1—O4^{i}	2.410 (14)
O2—Ca2	2.54 (2)	Ca1—O4^{vii}	2.410 (15)
O3—P1	1.627 (9)	Ca1—P1^{i}	3.48 (3)
O3—P2	1.680 (16)	Ca1—Ca1^{ii}	3.61 (2)
O3—Ca2^{iii}	2.968 (18)	Ca1—Ca1^{vi}	3.61 (2)
O4—P1	1.546 (15)	Ca1—Ca2^{vi}	3.79 (3)
O4—Ca1^{i}	2.410 (14)	Ca1—Ca2	3.81 (3)
O4—Ca1^{iv}	2.410 (15)	Ca2—O5^{viii}	2.33 (3)
O5—P2	1.530 (9)	Ca2—O6^{iii}	2.34 (2)
O5—Ca2^{v}	2.33 (3)	Ca2—O1^{i}	2.388 (18)
O6—P2	1.524 (11)	Ca2—O7^{vi}	2.427 (18)
O6—Ca2^{iii}	2.34 (2)	Ca2—O8^{ii}	2.554 (16)
O7—P2	1.53 (2)	Ca2—O3^{iii}	2.968 (18)
O7—Ca1^{ii}	2.37 (2)	Ca2—P2^{iii}	3.33 (2)
O7—Ca2^{ii}	2.427 (18)	Ca2—P2^{vi}	3.48 (3)
O8—Ca1	2.49 (2)	Ca2—P2^{viii}	3.50 (3)
O8—Ca2^{vi}	2.554 (16)	Ca2—Ca1^{ii}	3.79 (3)
P1—Ca1^{i}	3.48 (3)		

P1—O1—Ca2^{i}	138.9 (4)	O2—Ca1—Ca1^{vi}	142.3 (4)
P1—O1—Ca1	95.6 (5)	O8—Ca1—Ca1^{vi}	95.7 (3)
Ca2^{i}—O1—Ca1	120.4 (6)	O1—Ca1—Ca1^{vi}	113.63 (15)
P1—O2—Ca1^{ii}	131.1 (5)	P1^{i}—Ca1—Ca1^{vi}	63.5 (3)
P1—O2—Ca1	97.7 (4)	Ca1^{ii}—Ca1—Ca1^{vi}	150.2 (4)
Ca1^{ii}—O2—Ca1	95.7 (6)	O7^{vi}—Ca1—Ca2^{vi}	126.4 (5)
P1—O2—Ca2	123.3 (6)	O2^{vi}—Ca1—Ca2^{vi}	41.3 (4)
Ca1^{ii}—O2—Ca2	100.4 (8)	O4^{i}—Ca1—Ca2^{vi}	95.8 (7)
Ca1—O2—Ca2	98.9 (6)	O4^{vii}—Ca1—Ca2^{vi}	85.6 (6)
P1—O3—P2	132.7 (4)	O2—Ca1—Ca2^{vi}	154.58 (16)
P1—O3—Ca2^{iii}	138.8 (5)	O8—Ca1—Ca2^{vi}	41.9 (4)
P2—O3—Ca2^{iii}	86.9 (4)	O1—Ca1—Ca2^{vi}	109.3 (5)
P1—O4—Ca1^{i}	121.7 (5)	P1^{i}—Ca1—Ca2^{vi}	115.9 (6)
P1—O4—Ca1^{iv}	140.2 (4)	Ca1^{ii}—Ca1—Ca2^{vi}	125.0 (3)
Ca1^{i}—O4—Ca1^{iv}	96.9 (6)	Ca1^{vi}—Ca1—Ca2^{vi}	62.0 (3)
P2—O5—Ca2^{v}	129.1 (4)	O7^{vi}—Ca1—Ca2	37.8 (3)
P2—O6—Ca2^{iii}	117.4 (4)	O2^{vi}—Ca1—Ca2	122.2 (6)
P2—O7—Ca1^{ii}	132.2 (7)	O4^{i}—Ca1—Ca2	77.1 (6)
P2—O7—Ca2^{ii}	121.6 (4)	O4^{vii}—Ca1—Ca2	95.2 (6)
Ca1^{ii}—O7—Ca2^{ii}	105.4 (8)	O2—Ca1—Ca2	41.2 (3)
Ca1—O8—Ca2^{vi}	97.6 (7)	O8—Ca1—Ca2	154.8 (3)
O1—P1—O4	115.1 (4)	O1—Ca1—Ca2	84.7 (7)
O1—P1—O2	106.6 (3)	P1^{i}—Ca1—Ca2	60.6 (6)
O4—P1—O2	112.9 (5)	Ca1^{ii}—Ca1—Ca2	61.4 (2)
O1—P1—O3	109.5 (6)	Ca1^{vi}—Ca1—Ca2	104.5 (3)
O4—P1—O3	105.5 (6)	Ca2^{vi}—Ca1—Ca2	163.2 (2)
O2—P1—O3	106.9 (5)	O5^{viii}—Ca2—O6^{iii}	84.4 (7)

O1—P1—Ca1^{i}	83.6 (6)	O5^{viii}—Ca2—O1^{i}	119.5 (6)
O4—P1—Ca1^{i}	36.1 (4)	O6^{iii}—Ca2—O1^{i}	89.8 (5)
O2—P1—Ca1^{i}	109.0 (4)	O5^{viii}—Ca2—O7^{vi}	91.2 (7)
O3—P1—Ca1^{i}	136.0 (5)	O6^{iii}—Ca2—O7^{vi}	171.85 (18)
O6—P2—O7	111.4 (6)	O1^{i}—Ca2—O7^{vi}	86.5 (6)
O6—P2—O5	116.2 (6)	O5^{viii}—Ca2—O2	153.8 (2)
O7—P2—O5	112.5 (5)	O6^{iii}—Ca2—O2	114.7 (7)
O6—P2—O3	100.9 (4)	O1^{i}—Ca2—O2	80.1 (6)
O7—P2—O3	107.1 (4)	O7^{vi}—Ca2—O2	71.8 (8)
O5—P2—O3	107.7 (6)	O5^{viii}—Ca2—O8^{ii}	78.5 (7)
O6—P2—Ca2^{iii}	38.6 (4)	O6^{iii}—Ca2—O8^{ii}	108.1 (5)
O7—P2—Ca2^{iii}	114.8 (5)	O1^{i}—Ca2—O8^{ii}	156.5 (3)
O5—P2—Ca2^{iii}	132.4 (7)	O7^{vi}—Ca2—O8^{ii}	77.6 (6)
O3—P2—Ca2^{iii}	62.9 (5)	O2—Ca2—O8^{ii}	78.6 (8)
O6—P2—Ca2^{ii}	89.1 (7)	O5^{viii}—Ca2—O3^{iii}	113.1 (4)
O7—P2—Ca2^{ii}	36.4 (4)	O6^{iii}—Ca2—O3^{iii}	54.0 (3)
O5—P2—Ca2^{ii}	100.3 (7)	O1^{i}—Ca2—O3^{iii}	110.9 (8)
O3—P2—Ca2^{ii}	141.8 (4)	O7^{vi}—Ca2—O3^{iii}	134.2 (3)
Ca2^{iii}—P2—Ca2^{ii}	114.4 (6)	O2—Ca2—O3^{iii}	70.3 (4)
O6—P2—Ca2^{v}	85.8 (7)	O8^{ii}—Ca2—O3^{iii}	70.7 (7)
O7—P2—Ca2^{v}	135.3 (6)	O5^{viii}—Ca2—P2^{iii}	100.1 (7)
O5—P2—Ca2^{v}	31.1 (2)	O6^{iii}—Ca2—P2^{iii}	23.99 (16)
O3—P2—Ca2^{v}	109.5 (6)	O1^{i}—Ca2—P2^{iii}	97.6 (7)
Ca2^{iii}—P2—Ca2^{v}	104.2 (8)	O7^{vi}—Ca2—P2^{iii}	164.04 (14)
Ca2^{ii}—P2—Ca2^{v}	108.0 (8)	O2—Ca2—P2^{iii}	93.7 (7)
O7^{vi}—Ca1—O2^{vi}	85.2 (8)	O8^{ii}—Ca2—P2^{iii}	93.5 (7)
O7^{vi}—Ca1—O4^{i}	79.1 (5)	O3^{iii}—Ca2—P2^{iii}	30.3 (2)
O2^{vi}—Ca1—O4^{i}	84.4 (6)	O5^{viii}—Ca2—P2^{vi}	69.8 (9)
O7^{vi}—Ca1—O4^{vii}	81.7 (7)	O6^{iii}—Ca2—P2^{vi}	154.1 (3)
O2^{vi}—Ca1—O4^{vii}	81.6 (7)	O1^{i}—Ca2—P2^{vi}	101.3 (7)
O4^{i}—Ca1—O4^{vii}	157.0 (3)	O7^{vi}—Ca2—P2^{vi}	22.0 (2)
O7^{vi}—Ca1—O2	74.0 (6)	O2—Ca2—P2^{vi}	90.4 (9)
O2^{vi}—Ca1—O2	155.4 (3)	O8^{ii}—Ca2—P2^{vi}	69.2 (6)
O4^{i}—Ca1—O2	103.9 (7)	O3^{iii}—Ca2—P2^{vi}	138.1 (2)
O4^{vii}—Ca1—O2	82.6 (6)	P2^{iii}—Ca2—P2^{vi}	161.11 (12)
O7^{vi}—Ca1—O8	163.91 (19)	O5^{viii}—Ca2—P2^{viii}	19.8 (2)
O2^{vi}—Ca1—O8	82.9 (8)	O6^{iii}—Ca2—P2^{viii}	83.1 (7)
O4^{i}—Ca1—O8	110.4 (5)	O1^{i}—Ca2—P2^{viii}	99.6 (7)
O4^{vii}—Ca1—O8	85.9 (7)	O7^{vi}—Ca2—P2^{viii}	90.3 (7)
O2—Ca1—O8	114.6 (5)	O2—Ca2—P2^{viii}	162.09 (16)
O7^{vi}—Ca1—O1	121.9 (8)	O8^{ii}—Ca2—P2^{viii}	97.6 (8)
O2^{vi}—Ca1—O1	145.2 (3)	O3^{iii}—Ca2—P2^{viii}	125.3 (4)
O4^{i}—Ca1—O1	80.6 (4)	P2^{iii}—Ca2—P2^{viii}	104.1 (7)
O4^{vii}—Ca1—O1	120.7 (5)	P2^{vi}—Ca2—P2^{viii}	72.0 (8)
O2—Ca1—O1	59.4 (3)	O5^{viii}—Ca2—Ca1^{ii}	116.9 (5)
O8—Ca1—O1	73.4 (8)	O6^{iii}—Ca2—Ca1^{ii}	121.9 (6)
O7^{vi}—Ca1—P1^{i}	75.4 (7)	O1^{i}—Ca2—Ca1^{ii}	116.9 (4)
O2^{vi}—Ca1—P1^{i}	105.8 (6)	O7^{vi}—Ca2—Ca1^{ii}	66.3 (6)

O4^{i}—Ca1—P1^{i}	22.21 (12)	O2—Ca2—Ca1^{ii}	38.3 (4)
O4^{vii}—Ca1—P1^{i}	155.12 (17)	O8^{ii}—Ca2—Ca1^{ii}	40.5 (4)
O2—Ca1—P1^{i}	81.9 (6)	O3^{iii}—Ca2—Ca1^{ii}	68.1 (5)
O8—Ca1—P1^{i}	118.3 (7)	P2^{iii}—Ca2—Ca1^{ii}	98.3 (6)
O1—Ca1—P1^{i}	66.1 (4)	P2^{vi}—Ca2—Ca1^{ii}	73.8 (6)
O7^{vi}—Ca1—Ca1^{ii}	70.3 (2)	P2^{viii}—Ca2—Ca1^{ii}	133.8 (5)
O2^{vi}—Ca1—Ca1^{ii}	119.3 (6)	O5^{viii}—Ca2—Ca1	127.8 (3)
O4^{i}—Ca1—Ca1^{ii}	138.3 (4)	O6^{iii}—Ca2—Ca1	146.5 (6)
O4^{vii}—Ca1—Ca1^{ii}	41.6 (3)	O1^{i}—Ca2—Ca1	67.5 (4)
O2—Ca1—Ca1^{ii}	41.2 (4)	O7^{vi}—Ca2—Ca1	36.8 (6)
O8—Ca1—Ca1^{ii}	106.5 (2)	O2—Ca2—Ca1	39.9 (4)
O1—Ca1—Ca1^{ii}	92.1 (4)	O8^{ii}—Ca2—Ca1	89.7 (6)
P1^{i}—Ca1—Ca1^{ii}	119.1 (3)	O3^{iii}—Ca2—Ca1	110.1 (4)
O7^{vi}—Ca1—Ca1^{vi}	82.9 (3)	P2^{iii}—Ca2—Ca1	131.6 (6)
O2^{vi}—Ca1—Ca1^{vi}	43.1 (3)	P2^{vi}—Ca2—Ca1	58.5 (7)
O4^{i}—Ca1—Ca1^{vi}	41.6 (4)	P2^{viii}—Ca2—Ca1	123.4 (4)
O4^{vii}—Ca1—Ca1^{vi}	123.5 (5)	Ca1^{ii}—Ca2—Ca1	56.6 (5)

Symmetry codes: (i) $-x+1, -y+1, -z+1$; (ii) $-x+3/2, y-1/2, -z+3/2$; (iii) $-x+1, -y, -z+1$; (iv) $x-1/2, -y+1/2, z-1/2$; (v) $x-1/2, -y+1/2, z+1/2$; (vi) $-x+3/2, y+1/2, -z+3/2$; (vii) $x+1/2, -y+1/2, z+1/2$; (viii) $x+1/2, -y+1/2, z-1/2$.